We are IntechOpen, the world's leading publisher of Open Access books
Built by scientists, for scientists

6,900
Open access books available

186,000
International authors and editors

200M
Downloads

154
Countries delivered to

Our authors are among the

TOP 1%
most cited scientists

12.2%
Contributors from top 500 universities

CLARIVATE ANALYTICS
BOOK CITATION INDEX
INDEXED

WEB OF SCIENCE™

Selection of our books indexed in the Book Citation Index
in Web of Science™ Core Collection (BKCI)

Interested in publishing with us?
Contact book.department@intechopen.com

4

Multi-Well Engineered Heart Tissue for Drug Screening and Predictive Toxicology

Alexandra Eder, Arne Hansen and Thomas Eschenhagen
Department of Experimental Pharmacology and Toxicology,
University Medical Centre Hamburg-Eppendorf,
Germany

1. Introduction

Drug development is time- and cost-intensive and, overall, inefficient. Only one out of an estimated 10.000 new chemical entities (NCEs) finally enters the market. The later the failure occurs, the higher are the costs. It is for this reason that preclinical development aims at identifying the potential for failure as early as possible and with high sensitivity. On the other hand, high sensitivity generally also means low specificity, suggesting that many potentially successful NCEs are currently excluded from further development. Common reasons for exclusion are adverse drug reactions (ADR). Among the various ADRs, cardiac toxicities and arrhythmias play an important role, because they represent about 21% of all ADRs (Lasser et al., 2002) and are frequently lethal. The single most important mechanism in this context is the prolongation of cardiac repolarization bearing a proarrhythmic potential. These interferences can be visualized by standard ECGs as a prolongation of the QT-interval. Such a prolongation is called "long QT-syndrome" (LQT-syndrome) and is associated with *Torsade-de-Pointes* (TdP) arrhythmias and sudden cardiac death. In the past, several prominent drugs had to be withdrawn from the market due to TdP in humans, e.g. astemizole, terfenadine, cisapride, sparfloxacin, grepafloxacin and recently clobutinol (Silomat). Moreover, numerous drugs are still on the market that are associated with the potential to cause LQT and TdP, including widely prescribed drugs such as the antibiotic erythromycin.

Given the fatal consequences of LQT and TdP in healthy patients without any cardiac disposition, the regulatory bodies (FDA, EMEA and others) have decided some years ago to require testing for LQT to be an obligatory part of preclinical development of any NCE. Several tests have been developed and some of them are routinely used. The three major (but by far not exclusive) tests in the field are the HERG test, rabbit Purkinje fibers and telemetry in dogs. These tests have different advantages and disadvantages and are generally employed subsequently. The HERG test can be considered an obligatory test for all NCEs and it is unlikely that any company further develops a compound that showed major inhibitory activity in this test (of a single ion channel activity). However, examples exist of successful drugs on the market that are potent inhibitors of the HERG current without ever giving rise to TdP arrhythmia (e.g. verapamil, azithromycin). Thus, the predictive value of the HERG test is limited. Reasons lie, among others, in its inability to

give an integrated readout of effects of drugs on the electrophysiology of the intact cardiac myocyte or the intact heart as a multicellular organ consisting of a functional syncytium of cardiac myocytes and all other cardiac cell types that make up normal heart tissue (e.g. fibroblasts, endothelial cells and smooth muscle cells).

1.1 Cardiac tissue engineering

Over the past decade, techniques have been developed to generate cardiac tissue-like 3-dimensional constructs *in vitro* (Eschenhagen & Zimmermann, 2005). The field of cardiac tissue engineering opened the possibility for many applications. Artificial hart constructs may serve as means for cell-based cardiac repair and as improved *in vitro* models for predictive toxicology and target validation, taking advantage of a more physiological cellular environment. Previous studies used different approaches to construct engineered tissues: Cell seeding onto solid, preformed scaffolds (Carrier et al., 1999; Engelmayr et al., 2008; Leor et al., 2000; Li et al., 2000; Ott et al., 2008; Radisic et al., 2004), matrix-free generation of tissues from stackable cell sheets (Shimizu et al., 2002) or the generation of constructs in preformed casting moulds using hydrogels such as collagen I, matrigel, fibronectin or fibrin (Bian et al., 2009; Eschenhagen et al., 1997; Huang et al., 2007; Naito et al., 2006; Zimmermann et al., 2002). The hydrogel technique has been shown to be suitable for both, cardiac repair *in vivo* (Zimmermann et al., 2006) and target validation *in vitro* (El-Armouche et al., 2007). Circular engineered heart tissues (EHTs) were made by casting neonatal rat heart cells, collagen I and matrigel into circular casting moulds and develop a high degree of cellular differentiation, longitudinal orientation, intercellular coupling and force generation (Zimmerman et al., 2002). It turned out that several factors improve tissue quality and force generation of EHT such as phasic (Fink et al., 2000) or auxotonic stretch, increased ambient oxygen concentration during culture and supplementation with insulin (Zimmermann et al., 2006). Others demonstrated beneficial effects of electrical stimulation (Radisic et al., 2004). The possibility to generate cardiac myocytes from human embryonic stem cells (Kehat et al., 2001) or induced pluripotent stem cells (Zhang et al., 2009) have opened the realistic and exciting perspective to use these techniques for the validation of hypotheses and testing drugs in healthy and diseased human heart muscles (Zimmermann & Eschenhagen 2007).

The current techniques to generate engineered cardiac tissues are either not suitable for this purpose (stacked cell sheet technique) or exhibit drawbacks that limit their usefulness. Extensive handling steps preclude routine execution of large series in an at least medium through put scale and are always a source of variability. Furthermore, the EHT technique in the ring format requires relatively high numbers of cells and turned out to be difficult to miniaturize.

In this chapter we describe a new EHT technique that was driven by the intention to miniaturize the EHT-format for multi-well-testing and automated evaluation and to determine the suitability of EHTs for drug screening and predictive toxicology. The main results have been published in a recent original paper (Hansen et al. 2010). An essentiel change was to use fibrin(ogen) instead of collagen I as a matrix. Fibrinogen is part of the blood clotting cascade. It is a glycoprotein with a size of 340 kDa. Physiologically it achieves plasma concentrations of 1.5 to 4 g/l and can be relative easily purified from different species. An important mechanical property is its nonlinear elasticity. Due to this, fibrin polymers have a high elastic modulus under shear stress combined with a beneficial

softness in comparison to other filamentous biopolymers (Janmey et al., 2009). The final properties of fibrin are mainly governed by the concentrations of fibrinogen and thrombin. Additionally fibrin properties can be affected by the introduction of bonds by plasma transglutaminase (factor XIII; Janmey et al., 2009). In contrast to other extracellular matrices, the *in vitro* polymerisation of fibrin is very close to the *in vivo* fibrin polymer. Fibrin gels are fully degradable by fibrinolytic enzymes like plasmin. All together, the mechanical and biological properties, its availability from autologous sources in addition to the possibility to covalently bind growth or other factors (Hubbell 2003) make fibrin an interesting compound for tissue engineering approaches.

2. Methods

2.1 Cell isolation
Total heart cells (excluding the atria) were isolated from neonatal Wistar rats (postnatal day 0 to 3) by a fractionated DNase/Trypsin digestion protocol as previously described (Eschenhagen & Zimmermann, 2005). The resulting cell populations were immediately subjected to FBME generation. Experimental procedures were reviewed and approved by Ethics Committee, Hamburg University.

2.2 Manufacturing teflon spacers and sylgard posts racks
For the generation of fibrin-based mini-EHTs (FBMEs), Teflon spacer and silicone post racks were used. The Teflon spacers were important for the casting molds. They had the following geometry (Figure: 1B): length 12 mm, width 3 mm, height 13.5 mm. Sylgard 184 silicone elastomer (Dow Corning) was used for the production of silicone post racks, which were needed for culturing the FBMEs. The silicone post racks were made in custom-made Teflon casting molds. According to the manufacture's instructions, the 2-component Sylgard 184 was degassed under vacuum conditions before casting. The final silicone post racks consisted of 4 pairs of posts, having a little plate at their end. The racks had the following geometry (Figure 1A): length/width of rack: 79x18.5 mm, length of posts 12 mm, diameter 1 mm, plate diameter 2 mm, distance (center-center) 8.5 mm. They were initially self-made and currently industrial-made. Silicone post racks can be autoclaved and reused for several times.

2.3 Generation of fibrin-based mini-EHTs
The reconstitution mixture for the generation of fibrin-based mini-EHTs was prepared on ice as follows (final concentration): 4.1×10^6 cells/ml, 5 mg/ml bovine fibrinogen (Sigma F4753, stock solution: 200 mg/ml in 0.9% NaCl supplemented with 0.5 µg/mg aprotinin), 3 U/ml bovine thrombin (Sigma T7513, stock solution: 100 U/ml). To ensure isotonic conditions, one additional fibrinogen and thrombin volume of 2x DMEM was added. Ordinary 24-well cell culture plates were used as casting molds. After 1.6 ml of sterile 2% agarose (Invitrogen 15510-027) in PBS was pipetted into each well, the Teflon spacers could be placed. After the agarose was solidified, the Teflon spacers were removed. The silicone posts racks were placed onto the cell culture dish with each pair of silicone posts reaching into one of the preformed casting molds (geometry: 12x3x4 mm). The reconstitution mix was carefully resuspended. For each FBME 100 µl of the mixture was mixed briefly with an appropriate volume of thrombin and pipetted into an agarose slot. To ensure complete polymerization of the fibrinogen, the constructs were placed into a humidified cell culture incubator (37 °C, 7% CO_2, 40% O_2) for 2 hours. Before transferring the silicone posts racks to

a new medium-filled culture plate, every construct was covered with DMEM (300 µl) to ease the removal. FBMEs were maintained in 37 °C, 7% CO_2, 40% O_2 in a humidified cell culture incubator. Media was changed on Mondays, Wednesdays and Fridays. FBME medium consisted of DMEM (Biochrom F0415) supplemented with 10% horse serum (Gibco 26050), 2% chick embryo extract (self-made), 1% penicillin/streptomycin (Gibco 15140), insulin (Sigma I9278, 10 µg/ml) and aprotinin (Sigma A1153, 33 µg/ml).
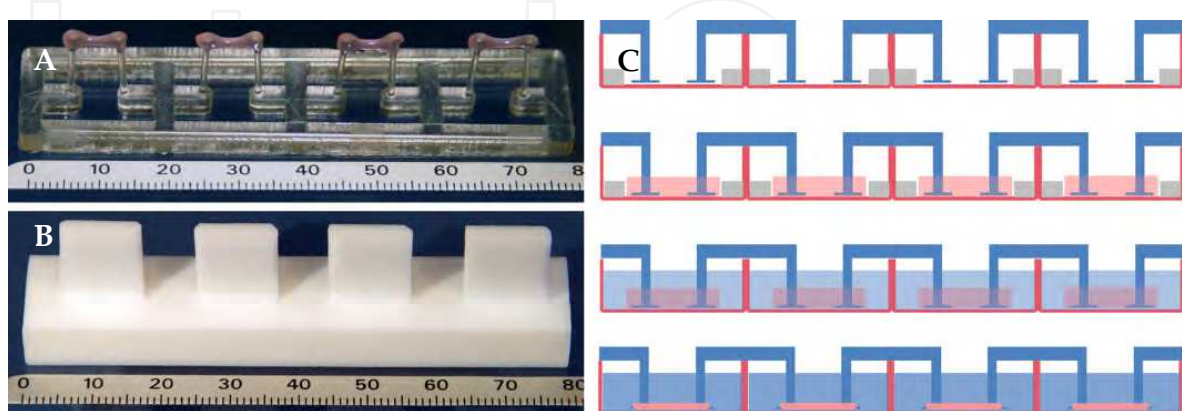

Fig. 1. Illustration of the experimental setup for casting and cultivation and photography of a silicone post rack with four FBMEs. Silicone post rack with four FBMEs (turned upside down, scale in millimetres; A). Teflon spacer for the generation of agarose casting molds (turned upside down, scale in millimetres; B). Illustration of FBME generation (C). First lane: Casting molds are made using Teflon spacers and agarose in a 24-well cell culture dish. Silicone posts racks are placed onto the culture dish, with each pair of posts reaching into a mold. Second lane: Mastermix is pipetted into each mold. Third lane: After 2 h the fibrin is polymerized and the silicone posts are embedded in the hydrogel. FBMEs can be transferred into a new medium-filled 24-well culture plate. Fourth lane: FBMEs are maintained in culture for 15 to 30 days (Hansen et al. 2010).

2.4 Video-optical analyses

The setup for video-optical analyses consisted of a cell culture incubator-like unit, in which gas conditions, humidity and temperature could be controlled. This device was equipped with a glass roof for monitoring purposes. A Basler CCD-camera (Type A 602f-2) was attached to an XYZ-device (IAI Corporation) and positioned above the glassroof in a PC-controlled manner. Light-emitting diodes (LEDs) were placed underneath the cell culture dish. Illumination of a single LED was synchronized with the video-optical recording procedure in order to minimize heating of the cell culture medium by LED waste heat. Figure 2A shows a schematic picture of the whole setup and 2B shows a 24 well cell culture plate with six silicone posts racks and with one FBME in every well (view from above). For the video-optical analyses a customized software package developed by Consulting Team Machine Vision (ctmv.de; Pforzheim, Germany) was used. This software is based on figure recognition and is able to identify the FBME's shape in a fully automated manner. In brief, the system automatically places measuring points at the top and bottom end of the contracting muscle strip. Due to the contraction, the distance in between the moving silicone posts changes. These changes are determined and recorded by the software over time. Based on post geometry, elastic modulus of the Sylgard 184 (2.6 kPa) and the delta value of post distance (post deflection), the developed force was calculated based on a recently published

equation (Vandenburgh et al. 2008). The recorded contractions are filtered and identified as such by certain peak criteria (e.g. threshold value, minimal force and minimum relaxation). Besides average force, the software calculates values for frequency, fractional shortening, contraction- and relaxation time (bpm, T1 and T2, respectively) based on the recognized contraction peaks. T1 and T2 were determined at 20% of peak maximum. Reports with an overview of the environmental information (temperature, gas, humidity) in the cell culture like unit plus all calculated parameters are automatically generated after each run. These underlie two levels of quality control: pictures are taken at the beginning and the end of each recording. Blue squares indicate top and bottom end of each respective FBME where the software placed the points for the measurement (Figure 2D). Contractions are recorded as force development over time. Identified peaks, which are included in the calculation, are marked with green squares (Figure 2C). The effort to analyse a 24-well plate with contracting muscle strips is limited to defining the XYZ-coordinates for each well once before starting a series of measurements.
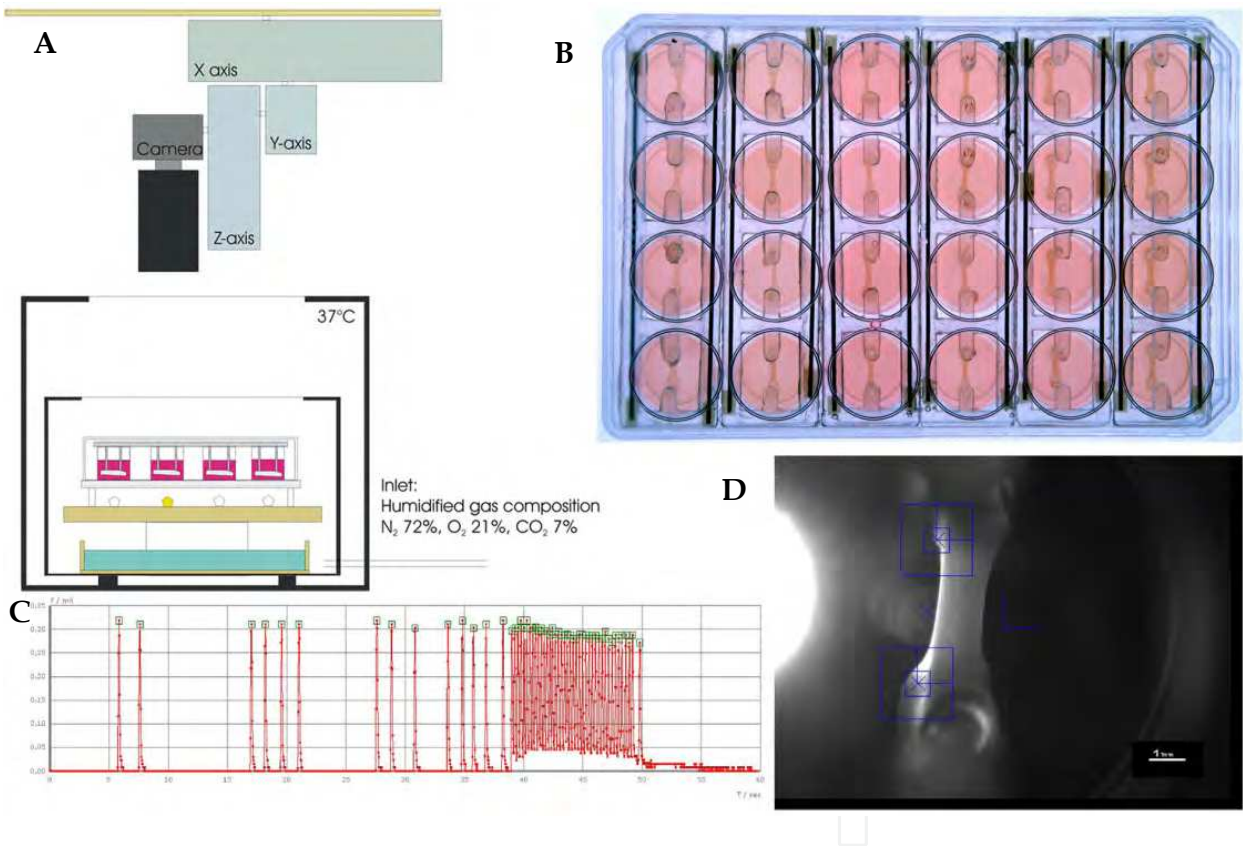

Fig. 2. Illustration of the experimental setup for video-optical recordings of FBME, a 24 well cell culture dish with FBMEs, a magnified view of a single FBME as recorded by the video camera and an example of a contraction pattern (one FBME for 60 s). A shows a schematic picture of the experimental setup for video-optical recordings. In B a 24 well cell culture dish with FBMEs is shown (view from above). The original contraction pattern of one FBME over time (60 s, C). Image of a contractile muscle strip from an automatically generated report (D). Blue squares indicate positions automatically recognized by the software at top and bottom end of the FBME. Green squares mark the recognized contraction peaks which are included for the calculation of several parameters (Hansen et al. 2010).

3. Results

3.1 General aspects of the new technique

We developed a new technique for the generation and evaluation of contractile cardiac tissue from neonatal rat heart cells *in vitro* (Hansen et al. 2010). In this method, isolated heart cells are mixed with fibrinogen, thrombin and medium and pipetted into rectangular casting moulds made from 2%-agarose in ordinary 24-well cell culture plates. Due to the polymerisation of the fibrin, the gel is fixed to both silicone posts. After 2 h at 37 °C the constructs can be transferred to new culture dishes and maintained under cell culture conditions for several days. Figure 1C demonstrates this procedure in a schematic way. During cultivation, the cells inside the gel spread along the force lines and form extensive cell-cell contacts, the hydrogel is remodelled and degraded. These processes are accompanied by marked condensation of the constructs and deflection of the silicone posts towards each other. The initial length of a FBME directly after casting is 8.5 mm and the mean final length 6.5 mm. The post deflection differs between individual FBMEs, likely reflecting their degree of cardiac tissue development. In consequence, each FBME is exposed to an "individually optimized preload". With this simplified method, 48-72 FBMEs can be routinely generated out of one cell preparation (30 rat hearts). Figure 2B illustrates a typical 24 well plate with silicone posts racks and FBMEs. Fibrin is affected by proteases in the culture medium. To decrease degradation, the protease inhibitor aprotinin at a concentration of 33 µg/ml is added to the medium. This inhibitor markedly reduces fibrinolysis but cannot entirely stop it. To further protect the hydrogel from proteolysis tranexamic acid, another protease inhibitor, can be added to the medium. The combination of both inhibitors results in improved stability and allows longer cultivation periods. Tranexamic acid-treated FBMEs have a markedly increased diameter (final width 1.3 to 1.4 mm [Figure 2C and 8D] instead of 0.2 to 1.0 mm in its absence [Figure 4A]).

3.2 Morphology and beating activity

Directly after casting, FBMEs appeared as a soft fibrin-block fixed at the end of the silicone posts and exhibiting the dimensions of the casting moulds (12x3xx mm). Within this clot, the heart cells were round and amorphous but homogeneously distributed throughout the gel (Figure 3A). During the first days after casting, cells spread, elongated along force lines, started to beat as single cells and finally in the form of synchronously beating areas on day 4 to 5. The further development was characterized by matrix remodelling and degradation. This lead to a marked reduction of the size (from 3 mm to 1-2 mm width in the presence and 0.2-1 mm in the absence of tranexamic acid) and increased cell-density. Between day 5 and day 7 the cardiomyocytes formed small groups (Figure 3B through E). Coherent beating of the muscle construct started around day 7 to 9. By day 10 the generated force was sufficient to rhythmically deflect the silicone posts. Measurements were routinely performed between day 14 to 16. At this point the cardiomyocytes finally appeared as spindle-shaped cells with an approximately length of 100 to 200 µm and a diameter of 10 to 20 µm (Figure 3F).

Hematoxylin/eosin-stained paraffin sections of mature FBMEs (day 15) showed a dense network of longitudinally aligned cells throughout the gel (Figure 4A). No clear evidence for cell density gradient from peripheral to central areas of the gel could be found, arguing against a significant inhomogeneity of oxygen and nutrient supply.
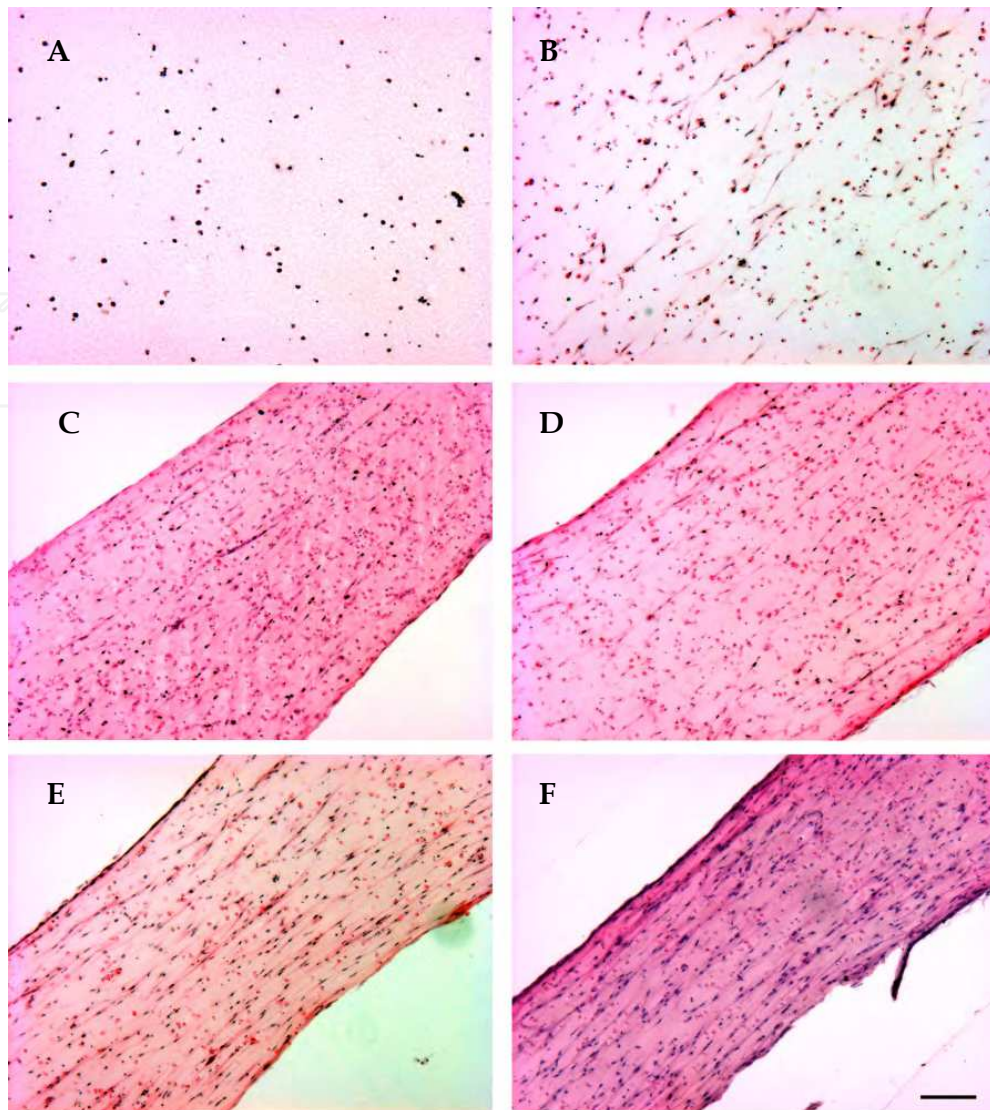
Fig. 3. Histological analysis of FBMEs. FBMEs were cultured with aprotinin plus tranexamic acid. For histological analysis they were fixed with formaldehyde at indicated time points, embedded with paraffin and the sections were HE-stained (10x magnification). A Day 0: cells are present as single, round and amorphous cell suspension in fibrin matrix; B day 3: cells spread out along force lines. C day 6, D day 9: degradation of extracellular matrix, cells spread and align with neighbouring cells. E day 12, F day 15: extended degradation of extracellular matrix, the cellular density is increased; cells align and show orientation along force lines. Scale bar 100 μm (Hansen et al. 2010).

Whole-mount FBMEs were also analysed by immunofluorescent staining. The pictures showed a dense network of regularly cross striated, α-actinin-positive, longitudinally aligned cardiomyocytes. The elongated cells had well developed sarcomeric structures reaching into the periphery of the cytoplasm. Cardiomyocytes were also characterized by connexion-43 positive structures, the gap junctions. In contrast to the *in vivo* situation connexion-positivity was mostly localized on lateral parts of the cell membrane, but not clustered at the border to connecting cells. Moreover, the immunfluorescence showed lectin-positive endothelial cells intermingled with cardiomycytes and forming primitive tube-like structures (Figure 4).
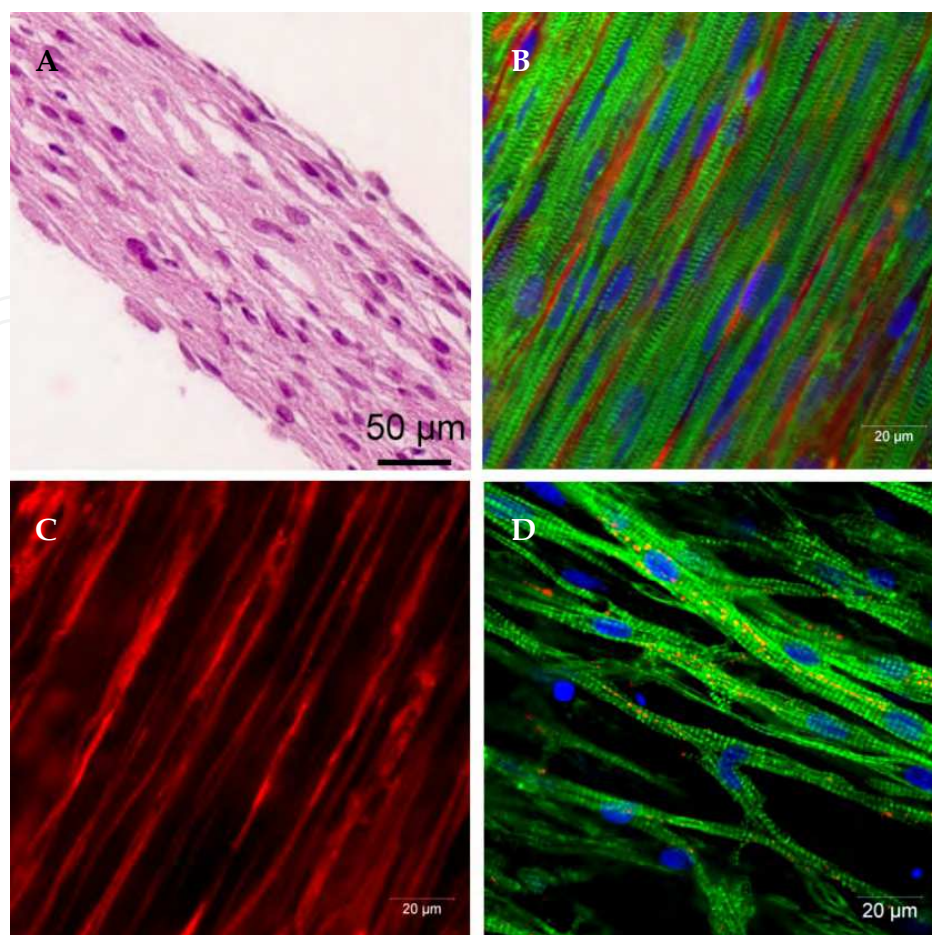
Fig. 4. Histological analysis of FBMEs (day 15, without tranexamic acid). A, HE-stained paraffin section. Note the almost complete absence of extracellular matrix and well-developed cardiac tissue structure. B, Merged immunofluorescence staining for α-actinin (green), lectin (red) and DRAQ5 (blue; 63x magnification). C, Lectin-positive structures alone (63x magnification). D, Connexin-43 (red), phalloidin (green) and DRAQ5 (blue; 63x magnification). Scale bar 50 μm (A) and 20 μM (B-D; Hansen et al. 2010).

3.3 DNA/RNA content, histone H3 phosphorylation and caspase-3 activity

To further investigate cell survival in FBMEs during culture, the histological data were supported by measurements on a molecular biological level. The DNA/RNA content, histone H3 phosphorylation as well as the caspase-3-activity were analysed. The DNA content dropped by 20% between day 0 and day 3. Thereafter it remained stable for at least two weeks (Figure 5A). Investigations of histone H3 phosphorylation as a marker of proliferative activity and caspase-3 activity as a marker for apoptosis in FBMEs were well in line with these observations. Histone H3 phosphorylation level was initially very low and further decreased over time (Figure 5C). Caspase-3 activity was high directly after cell preparation and dropped during culture even below detectable levels (Figure 5D). After an initial drop of the RNA-content during the first three days of 50% it remained, like the DNA content, more or less stable for at least two weeks (Figure 5B). In summary, these data suggest that some of the cells died within the first three days after casting, likely as a consequence of cell damage during the isolation procedure. Thereafter the cell population remained essentially stable in FBMEs.
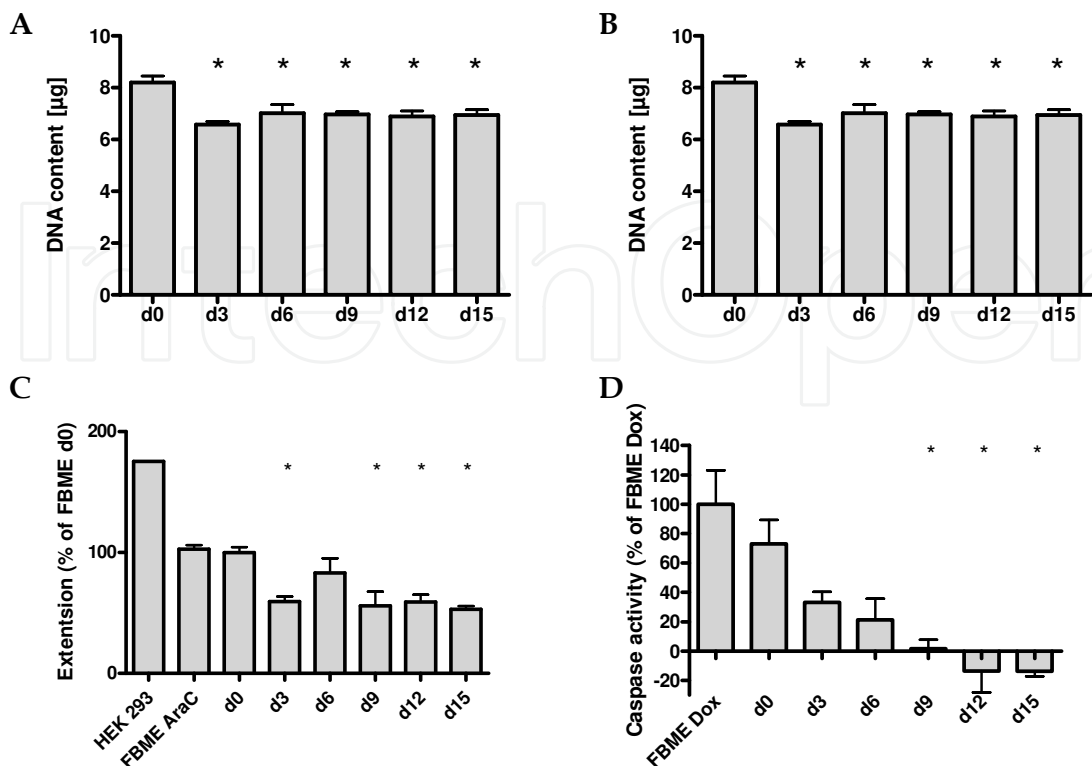
Fig. 5. DNA and total RNA content of FBMEs. A DNA content of FBMEs over time (n=4). B Total RNA content over time (n=4). * p<0.05 vs. d0 (Student's t test). Bars show means +/-SD. C, D Concentration of phosphorylated histone H3 (C) and caspase-3 activity (D) in FBMEs over time of cultivation. Day 0 represents freshly solidified FBMEs 2 h after casting. Proliferating HEK293 cells and AraC-treated FBMEs served as positive and negative controls for proliferation, respectively. Doxorubicin-treated FBMEs served as positive controls for caspase-3 activity. Bars show mean +/-SEM, n=4. * p<0.05 vs. d0 (Student's t test; Hansen et al. 2010).

3.4 Cardiac marker gene expression over time

To get an idea about cardiomyocyte maturation in FBMEs, transcript levels of known cardiac marker genes (α-actinin, SR Ca^{2+}-ATPase [SERCA], α- and β-myosin heavy chain [α-/β-MHC], Na^+/Ca^{2+}-exchanger [NCX], titin) were analysed over time. To avoid bias due to the effect of the drop of overall cell count after preparation, all values were normalized to the mRNA concentration of the cardiac myocyte-specific protein calsequestrin 2. Values were additionally compared to intact adult (ARH) and neonatal rat hearts (NRHT; Figure 6). In the first phase (day 0 to day 6), which represents the time when the single cells spread, formed clusters and started to beat, the transcript levels seemed to be relatively stable. In the second phase (day 9 to day 12) the expression levels reached their maximum concomitantly with the start of rhythmical deflection of the silicone posts by the FBMEs. In the third phase (day 12 to day 15) transcript levels generally decreased. Some cardiac markers (α-actinin, SERCA, α-MHC) reached a comparable level to native myocardium on day 15. Other (β-MHC, titin and NCX) remained several fold higher, indicating higher remodelling activity.
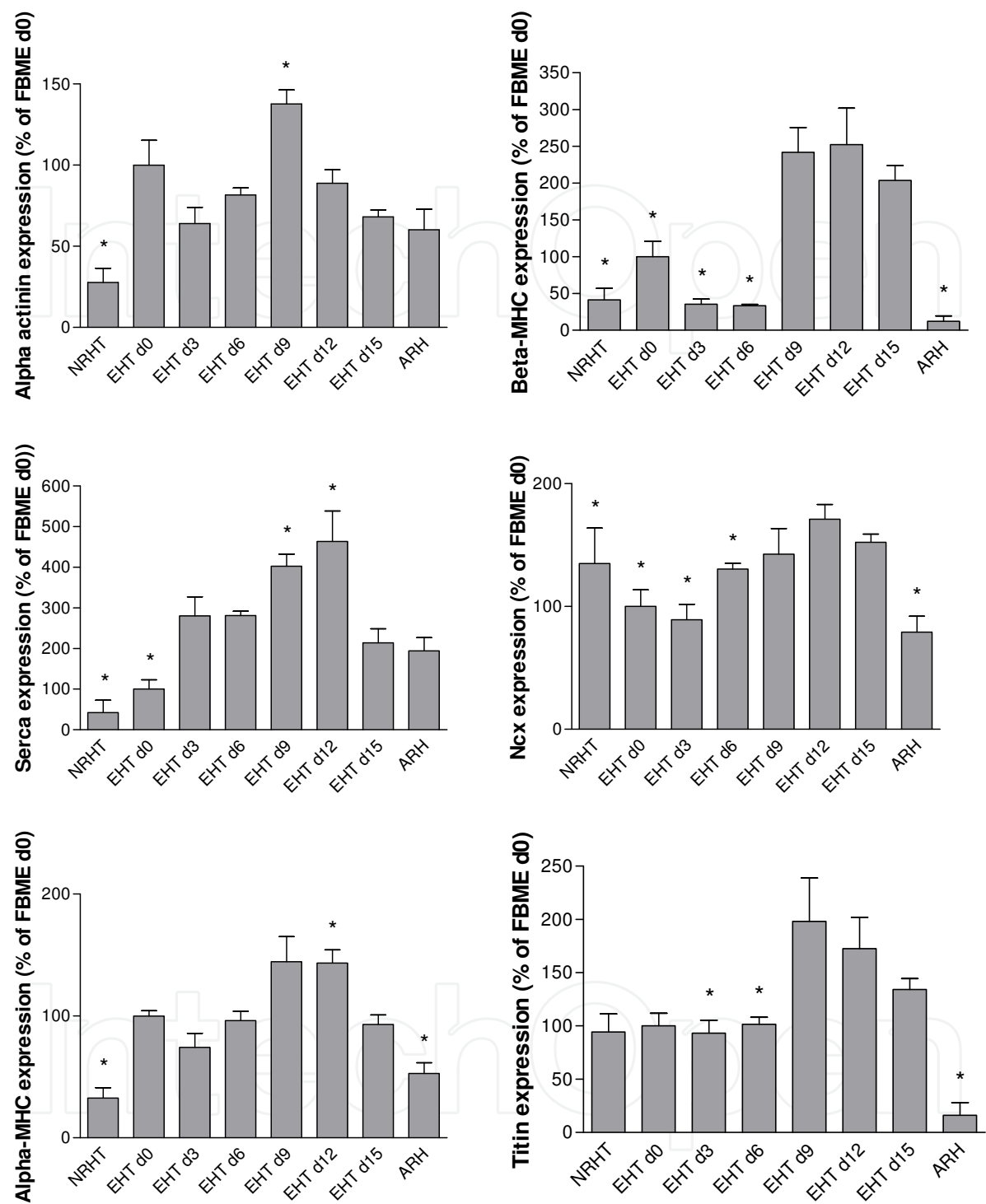
Fig. 6. RT-qPCR of FBMEs in comparison to neonatal (NRHT) and adult rat heart (ART). ΔΔCT values were generated by normalisation to the mRNA of cardiac specific protein calsequestrin 2 (average CT values for normalisation were as follows: d0: 20.8, d3: 20.4, d6: 20.6, d9: 21.3, d12: 21.6, d15: 20.5). Figures show relative expression compared to day 0. Each bar represents results from 4 biological replicates (each measured 3 times). * $p < 0.05$ vs. day 15 (Student's t test). Bars show means +/- SEM (Hansen et al. 2010).

3.5 Non quantitative ion channel expression profile

Ion channels play an important role as targets of proarrhythmic drugs. To determine whether the principal ion channel subunits known from human hearts are expressed in rat FBMEs transcripts of 23 ion channel α-subunits (7 calcium channels, 6 sodium channels, 10 potassium channels) were amplified from total RNA of FBMEs and a nonfailing human heart sample by RT-PCR (35 cycles). 22/23 transcripts were amplified from both sources, one channel (CacnA1I) was neither amplified in FBMEs nor in the nonfailing human heart (Figure 7).
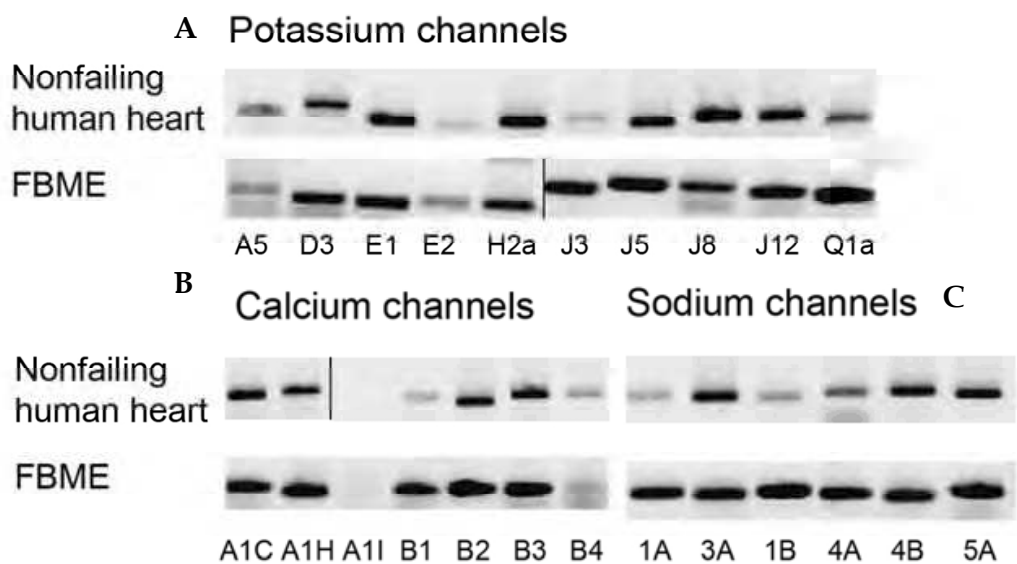

Fig. 7. Agarose gel of the PCR-products of 23 ion channel subunits. The ion channel profile of FBMEs was compared to the expression profile of a nonfailing human heart. Potassium channels (A), calcium channel (B) and sodium channels (C) showed qualitatively similar results (descriptions indicate the related gene for each channel subunit; for further information see table 1; Hansen et al. 2010).

3.6 Robustness and reproducibility of the new method

To determine robustness and reproducibility or the assay, we generated 6 independent series of FBMEs (1-2 24-well plates each, total number 192 FBMEs) and analysed them under standard conditions (culture medium with insulin, aprotinin and tranexamic acid; measurements done by video-optical recordings). Two FBMEs could not be transferred from the casting moulds, 4 FBMEs were not recognized by the software and 17 did not beat during the recording time (60 s) at day 15. Thus, the total success rate was 89% (169/192; Figure 8). Contraction parameters were examined and compared among different series. These results showed that the average force per series (day 15) was between 0.11 and 0.22 mN (series SD 7.6%), the contraction time (T1=time to peak) ranged between 66 and 81 ms (series SD 41%), relaxation time (T2=time to 80% relaxation) between 67 and 88 ms (series SD 25%), frequency between 162 and 20 beats per minute (series SD 109%), construct diameter between 1.3 and 1.4 mm (series SD 9.9%) and length between 5.6 and 6.7 mm (series SD 16.7%). The relatively large size in FBME diameter in these examinations could be attributed to the use of tranexamic acid.

Family	Abbre-viation	Description
KCN	A5	Voltage-gated channel subunit Kv1.5
	D3	Voltage-gated channel subunit Kv4.3
	E1	Potential voltage-gated channel subunit beta (KvLQT1; ERG; function: I_{Ks} or $_{Kr}$)
	E2	Potential voltage-gated channel subunit beta (minK-related peptide 1; KvLQT1; ERG; function: I_{Ks} or I_{Kr})
	H2a	I_{Kr} producing rapid voltage-gated channel subunit beta (ether-a-go-go-related gene (ERG) channel 1)
	J3	G protein-activated inward rectifier channel 1 (Kir3.1)
	J5	G protein-activated inward rectifier channel 4 (Kir3.4)
	J8	ATP-sensitive inward rectifier channel 8 (Kir6.1)
	J12	ATP-sensitive inward rectifier channel 12 (Kir2.2)
	Q1a	I_{Ks} producing slow voltage-gated channel subunit alpha (KvLQT1)
CACN	A1C	Voltage-dependent subunit alpha-1C (L-type)
	A1H	Voltage-dependent subunit alpha-1H (T-type)
	A1I	Voltage-dependent subunit alpha-1I (T-type)
	B1	Voltage-dependent subunit beta-1 (L-type)
	B2	Voltage-dependent subunit beta-2 (L-type)
	B3	Voltage-dependent subunit beta-3 (L-type)
	B4	Voltage-dependent subunit beta-4 (L-type)
SCN	1A	Voltage-gated channel protein type-1 subunit alpha
	3A	Voltage-gated channel protein type-3 subunit alpha
	1B	Voltage-gated channel subunit beta-1
	4A	Voltage-gated channel protein type 4 subunit alpha
	4B	Voltage-gated channel subunit beta-4
	5A	Voltage-gated channel protein type-5 subunit alpha

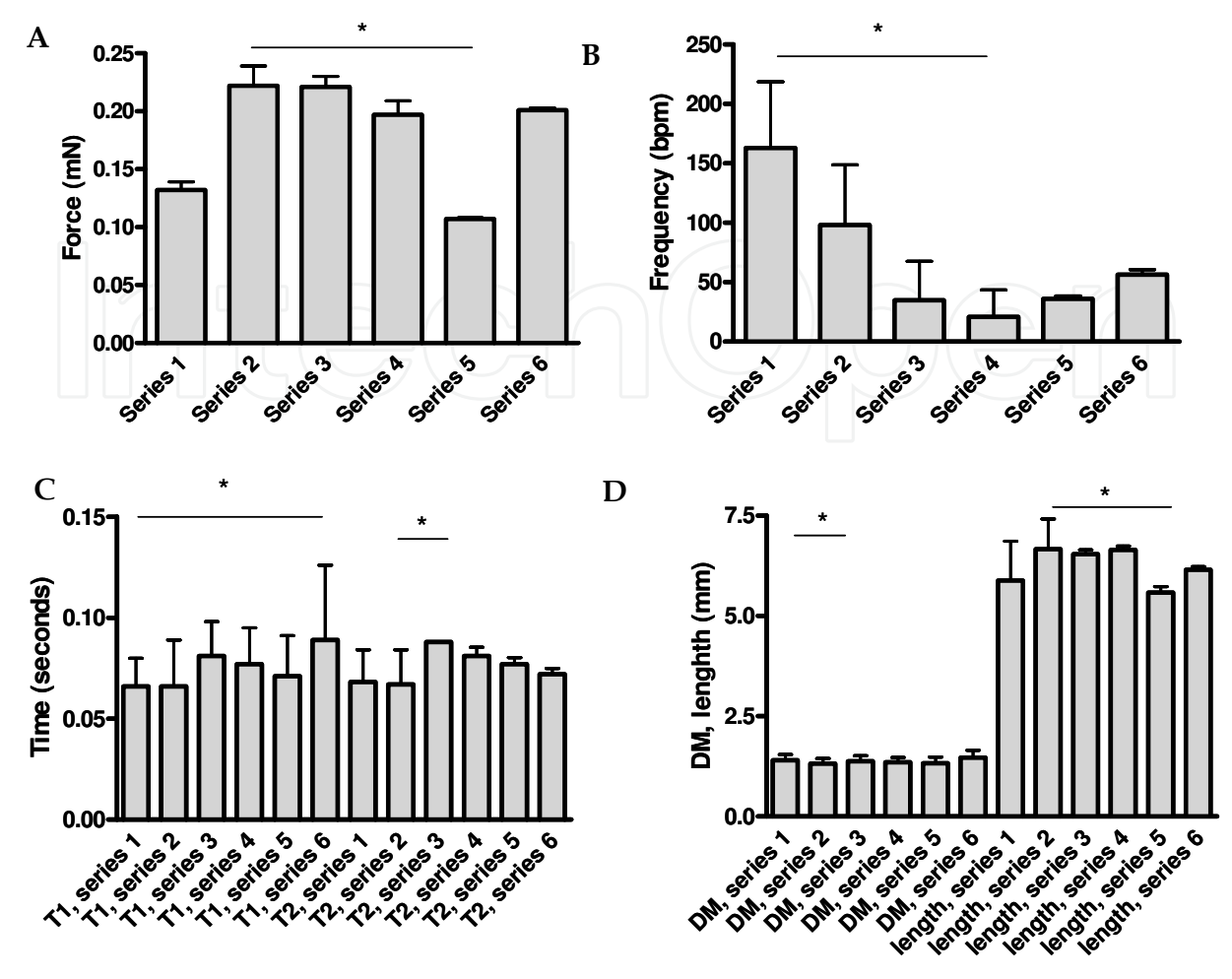Table 1. Overview of the analysed ion channels shown in figure 7.

Fig. 8. Reproducibility of the assay. FBMEs were generated at 6 different time points (series 1-6) and spontaneous activity was recorded on day 15. Parameters of contractility (A: force, B: frequency, C: contraction time T1, relaxation time T2) and construct dimensions (D) were averaged and compared. Minimal and maximal values were used to test for significant differences and are indicated with * $p<0.05$ (Student's t test). Bars show means +/- SD. Analysed FBMEs for each series were: Series 1: n=21, series 2: n=24, series 3: n=20, series 4: n=18, series 5: n=39, series 6: n=47 (Hansen et al. 2010).

3.7 Cardiotoxic and proarrhythmic effects of drugs

To determine whether the new method could be used for the detection of cardiotoxic and proarrhythmic drug effects, well characterized compounds with known cardiotoxic and repolarization-inhibitory effects were tested. The cardiotoxic drug doxorubicin was applied in different concentrations (0.1-1.000 nmol/L) for up to 96 h. Doxorubicin-treated FBMEs showed time- and concentration-dependent changes in contractile force. Very low concentrations of doxorubicin (1-10 nmol/L) led to a trend towards an increase in contractile force, 100 nmol/L induced a transient increase in contractile force after 24 h which was followed by a decrease at 72 and 96 h (Figure 9). In the presence of 1 μmol/L doxorubicin all FBMEs stopped to beat after 3 days.

To examine a repolarization-inhibitory effect on FBMEs, the experimental I_{Ks}-blocker chromanol 293B as well as the clinically used drugs quinidine and erythromycin were
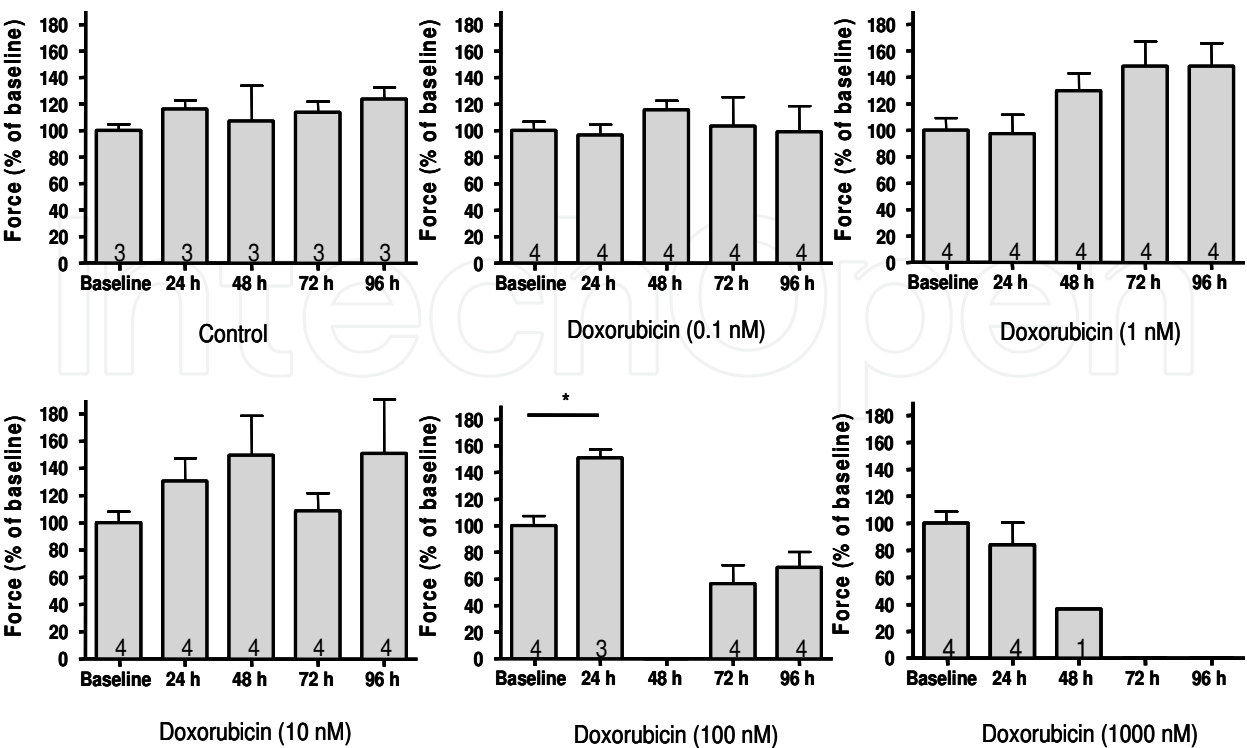
Fig. 9. Doxorubicin toxicity on FBMEs. FBMEs were incubated in the presence of doxorubicin (0.1-1000 nM, starting at day 13 of culture), average forces were determined daily. While doxorubicin at 0.1 µM increased force after 24 hours, higher concentrations (1 µM) lead to a time-dependent reduction in force development. * $p<0.05$ (Student's t test). Bars show means ⁻ +/- SEM, number of evaluated (beating) constructs as indicated (Hansen et al. 2010).

tested. All three compounds induced a concentration-dependent delay in relaxation time (T2; Figure 10). In the presence of chromanol 293B, FBMEs already showed a prolongation of T2 at a concentration of 1 µmol/L. At 100 µmol/L chromanol, T2 was 7-fold longer than control, resulting in a "church-like" configuration of the twith (Figure 10). Quinidine and erythromycin, both associated with arrhythmias in clinical applications, also extended the relaxation time at high concentrations (100 µmol/L). Time of contraction was not affected by any of the compounds.
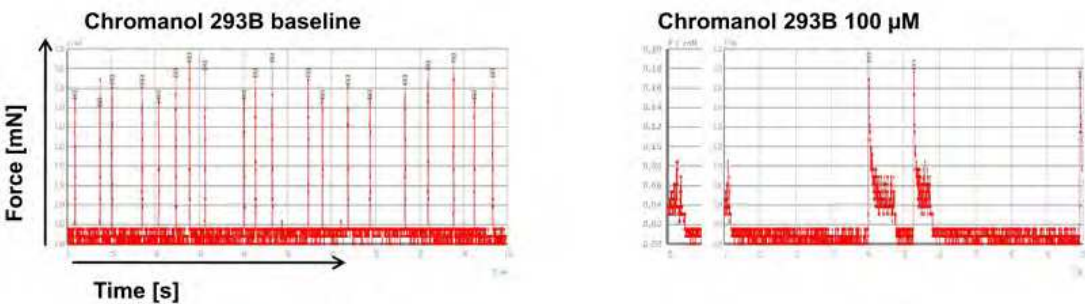

Fig. 10. Chromanol 293B-induced "church-like" contraction pattern. Cutout of the original contraction recordings in the presence and absence of Chromanol 293B (100 µM; modified from: Hansen et al. 2010).
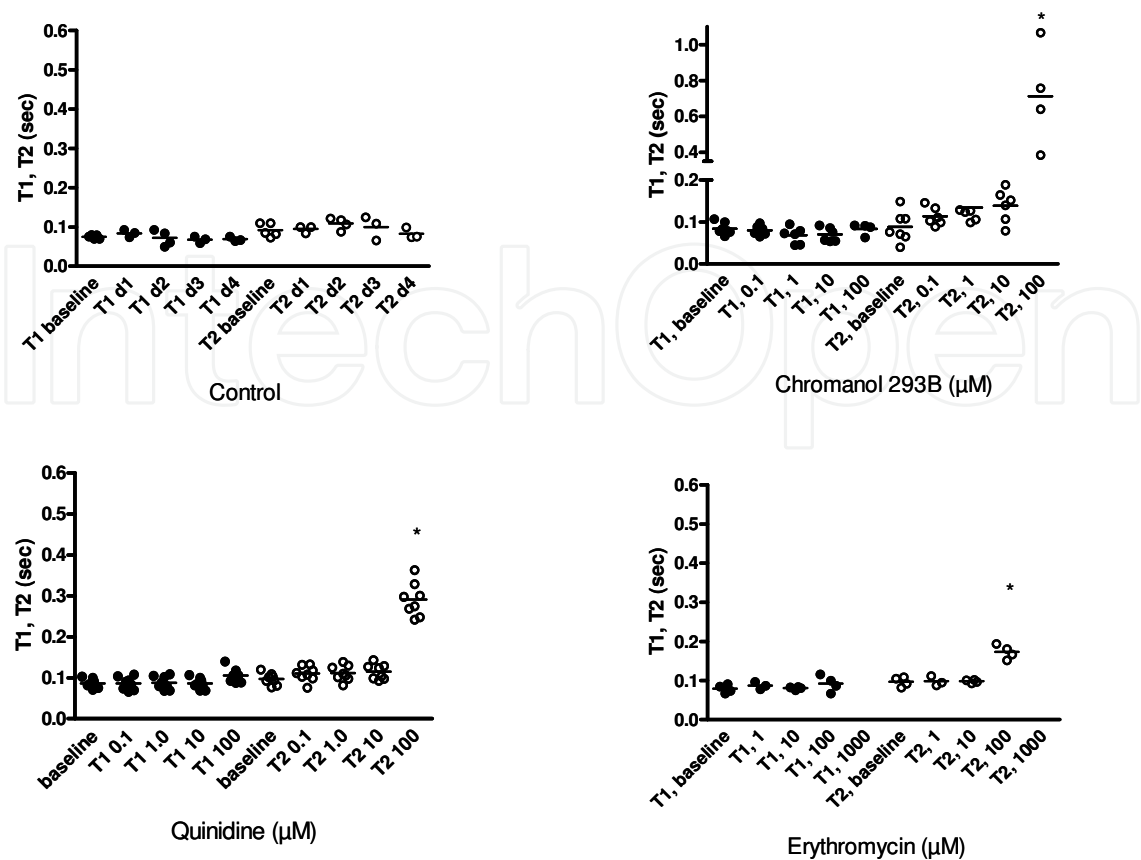
Fig. 11. Effect of repolarisation inhibitors on FBME contraction (T1) and relaxation time (T2). FBMEs were incubated with increasing concentrations of the indicated compounds (1-2 h) and evaluated before application of drug (baseline) and after each concentration. Note the absence of effect of all compounds on T1 and the concentration-dependent increase in T2 with chromanol, quinidine and erythromycin (at 1000 μM of erythromycin FBMEs discontinued contractile activity). A typical alteration of contraction peak morphology with increasing concentrations of quinidine, chromanol and erythromycin is shown in supplementary figure 5. * $p < 0.05$ (Student's t test). Bars show means +/- SEM, each spot represents one analysed FBME (Hansen et al. 2010).

4. Conclusion

In this book chapter we describe a recently developed method (Hansen et al. 2010) to generate miniaturized, fibrin-based EHTs (FBMEs) in a 24-well format and determine their contractile activity in an automated manner. This technique turned out to be robust and highly reproducible. Its main advantages are its simplicity in terms of handling, the standard 24-well format, its robustness and the high content automated readout of contractile activity. Compared to previously EHT-protocols (Eschenhagen et al. 1997, Zimmermann et al. 2002), three major changes were introduced. (i) Collagen I was replaced by fibrinogen and thrombin. Due to the fast fibrin-polymerisation, the heart cells were homogenously distributed throughout the entire hydrogel. Polymerisation occurs in minutes and allows transfer of the constructs from the casting moulds to a new medium-filled culture dish after two hours. Moreover, fast solidification allowed 50% higher cell concentration ($0.6 \times 10^6 / 150$ μl versus $2.5 \times 10^6 / 900$ μl), because it prevents accumulation of

cells at the bottom of the casting moulds with detrimental consequences. Fibrin has additional advantages for future applications, such as transplantations. It is available from autologoues sources and has the ability to couple covalently growth-promoting, angiogenic or other interesting factors (Hubble 2003). (ii) The original ring-format was changed to a stripe-format. This step was very important because it allowed miniaturization (volume reduced from 900 to 150 µl), the use of standard 24-well plates and automation. The silicone racks with 4 pairs of posts each allow simple transfer of FBMEs from one plate to another and thus reduce the number of nonstandardized handling steps to a minimum. Moreover, the silicone posts subject the growing muscle construct to an individually optimized preload and allow them to perform contractile work against the elastic properties of the post. (iii) Video-optical measurements of contractile parameters further improved the whole technique. They superseded the manual transfer for measurements as it was required in former EHT-protocols. Additionally, video-optical recordings allowed simple, reproducible, standardized measurements of large series in a short spell.

The new stripe-format was inspired by a previously described method for generating skeletal muscle tissues (Vandenburgh et al. 2008). Turning the silicone posts up side down was the major difference to this method and simplified handling. In this way the quality of the constructs could be determine with an ordinary microscope or even by eye and opened the possibility for automated video-optical recordings from above the plate. This experimental setup, in combination with fibrin, has several important features. (i) It is simple and not longer addicted to some kind of special dish because standard 24-well cell culture plates can be used. In the beginning silicone posts racks were self-made, which turned out to relevantly limit reproducibility. We therefore have the racks industrial made now, which makes the method robust and highly reproducible (Figure 8). (ii) FBMEs exhibit an excellent cardiac tissue development (Figure 4). Several factors are likely to contribute to these beneficial effects. As outlined above, the fast polymerisation of fibrin allowed higher cell concentrations and lead to homogenous cell distribution throughout the hydrogel. Another reason was that cell survival appeared very high in the current fibrin-based format. Moreover, proliferative activity (of non-myocytes) was very low (Figure 5), making the system stable over prolonged periods. The stable mRNA expression pattern of cardiac markers (α-actinin, α-MHC, titin, calsequestrin 2 and SERCA) may be an additional hint for a relatively stable system. Interestingly, the fetal gene marker β-MHC showed a several fold decrease within in the first six days. This phase was associated with cell spreading and contractions on a cellular level. Later, between day 6 and day 9 there was a ~5-fold increase of the β-MHC mRNA expression, coinciding with the beginning of macroscopic contractions. A third positive effect of the described new technique is the optimized mechanical load on the cardiomyocytes. The mechanical load is produced by the resistance of the silicon posts and adapted individually for each FBME. If the tonic (diastolic force) of the construct is high, post deflection by the FBMEs is stronger and *vice versa*. Furthermore, the FBMEs can perform contractile work against an elastic resistance. These circumstances mimic in some ways the *in vivo* situation in which the beating heart needs to work against the afterload induced by the total peripheric resistance. This kind of optimized "auxotonic" load in contrast to motorized phasic stretch improves tissue development as shown earlier in other EHT-studies (Zimmermann et al. 2006).

Regarding the development of a drug screening, miniaturization, reduction of nonstandardized steps during the procedure and an automated, objective readout were very important. The miniaturization to a 24-well format reduced the cell number by a factor of

~4. Additionally, pilot experiments could show that a further miniaturization to a 96-well format would be possible. At this point the 24-well format turned out to be a good compromise between miniaturization and ease of handling. FBMEs do not longer need to be manually transferred as single tissues because the entire silicon racks were handled. In contrast to that, circular EHTs needed to be manually transferred from the casting mould to a motorized stretcher and finally from the stretcher to the organ bath for the measurements. Compared to this method, the video-optical recordings were simple and robust. To confirm the calculated forces, isometric measurements were exemplarily done in the organ bath in parallel and showed that the calculated forces were roughly in the range of the measured ones (0.3 vs. 0.9 mN). The threefold difference could indicate a systematic error, but more likely reflects optimized conditions in the organ bath (preload optimization, electrical pacing and isometric versus auxotonic contraction). A force of 0.9 mN (organ bath) and a diameter of 0.2 mm (Figure 4A; without tranexamic acid) results in a relative force development of 28.7 mN/mm². This is still lower than values in an intact muscle (50 mN/mm²), but point in the right direction. The development of a software which works by automated figure recognition was important in two aspects. On the one hand, it is time-saving since it calculates all important contractile parameters automatically. On the other hand, it provides an objective readout.

Initial experiments to determine the suitability of FBMEs to detect either cardiotoxic or proarrhythmic effects looked promising. The known cardiotoxic drug doxorubicin suppressed contractile activity at the highest concentration (1.000 nmol/L) and increased force at lower concentrations (100 nmol/L) and earlier time points (24 h). This may be due to the reactive oxygen species-generating effect of this compound, which at later time points and/or higher concentrations turned into toxicity.

Three known proarrhythmic drugs caused a concentration-dependent prolongation of relaxation time in FBMEs. Chromanol 293B is an experimental I_{Ks}-blocker with an IC_{50}-value of 8 µmol/L in H9c2 cells (Lo et al. 2005). A concentration of 100 µmol/L was needed to fully block I_{Ks} in these cells. This correspond well to the relaxation-prolonging effect in FBMEs, which was visible at 10 µmol/L and marked at 100 µmol/L (Figure 10) matching quite well the published data (Lo et al. 2005). Quinidine, known as a class IA antiarrhythmic drug according to Vaughan-Williams classification (Vaughan-Williams 1975), also blocks I_{Ks} and I_{Kr} with EC_{50} values of 10 µmol/L and 300 nmol/L, respectively (Lo et al. 2005; Redfern et al. 2003). In FBMEs, quinidine prolonged relaxation time at 100 µmol/L. This is not an entirely different range in comparison with the determined IC_{50} for quinidine on I_{Ks} but far away from I_{Kr}-IC_{50}. This argues again for the role of I_{Ks} in FBME-repolarisation. Erythromycin, a clinically used antibiotic, which is associated with *Torsades-de-Pointes* arrhythmias and increased lethality in men (Ray et al. 2004), inhibits I_{Kr} but not I_{Ks} in dogs (Antzelevitch et al. 1996) and increases action potential duration in rat ventricular cardiomyocytes (IC_{50} 60 µmol/L; Hanada et al. 2003). In FBMEs erythromycin caused an increase in relaxation time at concentrations of 100 µmol/L and above. Even though the channel subunits for both I_{Kr} and I_{Ks} are expressed on mRNA-level in FBMEs (Figure 7), their role in repolarisation of rat cardiomyocytes is still controversial (Regan et al. 2005). In any case, the observation that the prototype proarrhythmic drugs specifically affected relaxation time in FBMEs indicates that this parameter may be useful as a surrogate of repolarisation. However, the detailed mechanisms behind the cardiotoxic and proarrhythmic effects are still unclear and need to be further investigated in follow up studies.

The presented technique still has a number of important limitations with regard to drug screening. (i) The cell preparation cannot be fully standardized. In particular, the age of newborn rats varies from 0-3 days and has significant impact of the quality of FBMEs, most likely explaining part of the variability between series (Figure 6). (ii) The system is not well suited to determine acute positive or negative inotropic effects because measurements are done under spontaneous beating, leading to confounding effects of concomitant negative or positive chronotropic effects. We are working on a system which allows measurements to be done under continuous pacing. (iii) Histological observations showed spindle-shaped cardiomyocytes and a predominantly lateral orientation of connexion-43-postive gap junctions. This suggests that cardiomyocytes, despite functional, molecular and morphological indices of advanced maturation, do not reach an adult phenotype. (iv) Our assay system exclusively monitors alterations in contractile activity and does not directly determine calcium transients or action potential duration. We believe that relaxation time is a good surrogate parameter of action potential, but the direct proof is still lacking. (v) Finally, rodents are known to be poor models for detecting proarrhythmic drug effects because mechanisms governing their action potential differ considerably from that in humans. For example, I_{Kr} plays a relatively minor role in rodents, but a major one in humans (Regan et al. 2005). Our present results suggest that proarrhythmic drug effects can still be monitored in this system, but much more work is necessary to determine which ion channel or combination of ion channels have to be blocked to see changes in relaxation time and/or arrhythmias in FBMEs.
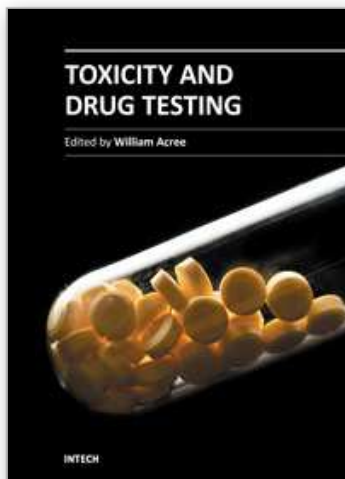
Thus, validation of the new system will require testing of a large number of drugs that are known to cause cardiac arrhythmias in humans and those that are known to be free of arrhythmic side effects, including those that have effects on HERG but are not associated with *Torsades-de-Pointes* arrhythmias. Moreover, a number of randomly chosen new chemical entities should be analysed to obtain an estimate how many non selected compounds give a signal. These studies are currently under way.

5. References

Antzelevitch, C.; Sun, Z. Q.; Zhang, Z. Q. & Yan, G. X (1996). Cellular and ionic mechanisms underlying erythromycin-induced long QT intervals and torsade de pointes. *Journal of the American College of Cardiology*; 28:1836-48

Bian, W.; Liau, B.; Badie, N. & Bursac, N. (2009). Mesoscopic hydrogel molding to control the 3D geometry of bioartificial muscle tissues. *Nature Protocols*; 4:1522-34

Carrier, R. L.; Papadaki, M.; Rupnick, M.; Schoen, F.J.; Bursac, N.; Langer, R.; Freed, L. E. & Vunjak-Novakovic, G. (1999). Cardiac tissue engineering: cell seeding, cultivation parameters, and tissue construct characterization. *Biotechnology Bioengineerening*; 64:580–589

El-Armouche A, Singh J, Naito H, Wittköpper K, Didié M, Laatsch A, Zimmermann WH, Eschenhagen T. (2007). Adenovirus-delivered short hairpin RNA targeting PKCalpha improves contractile function in reconstituted heart tissue. *Journal of Molecular Cell Cardiology*; 43:371-6

Engelmayr, G. C. Jr; Cheng, M.; Bettinger C. J.; Borenstein J.T.; Langer, R. & Freed L. E. (2008). Accordion-like honeycombs for tissue engineering of cardiac anisotropy. *Nature Materials*.; 7:1003–1010

Eschenhagen, T.; Fink, C.; Remmers, U.; Scholz, H.; Wattchow, J.; Weil J.; Zimmermann, W.; Dohmen, H. H.; Schafer, H.; Bishopric, N.; Wakatsuki, T. & Elson, E. L. (1997). Three-dimensional reconstitution of embryonic cardiac myocytes in a collagen matrix: a new heart muscle model system. *The FASEB Journal*; 11:683–694

Eschenhagen, T. & Zimmermann, W.H. (2005). Engineering myocardial tissue. *Circulation Research*.; 97:1220-31

Fink, C.; Ergün, S.; Kralisch, D.; Remmers, U.; Weil, J. & Eschenhagen, T. (2000). Chronic stretch of engineered heart tissue induces hypertrophy and functional improvement. *The FASEB Journal*; 14:669-79

Hanada, E.; Ohtani, H.; Hirota, M.; Uemura, N.; Nakaya, H.; Kotaki, H.; Sato, H.; Yamada, Y. & Iga, T. (2003). Inhibitory effect of erythromycin on potassium currents in rat ventricular myocytes in comparison with disopyramide. *The Journal of Pharmacy and Pharmacology*; 55:995-1002

Hansen, A.; Eder, A.; Bönstrup, B.; Flato, M.; Mewe, M.; Schaaf, S.; Aksehirlioglu, B.; Schwörer, A.; Uebeler, J. & Eschenhagen T. (2010). Development of a drug screening platform based on engineered heart tissue. *Circulation Research*; 107(1):35-44.

Huang, Y.C.; Khait, L. & Birla, R. K. (2007). Contractile three-dimensional bioengineered heart muscle for myocardial regeneration. *Journal of Biomedical Material Research Part A*; 80:719–731

Hubbell, J. A. (2003). Materials as morphogenetic guides in tissue engineering. *Current Opinion in Biotechnology*; 14:551-8

Janmey, P. A.; Winer, J. P. & Weisel, J.W. (2009). Fibrin gels and their clinical and bioengineering applications. *Journal of the Royal Society Interface*; 6:1-10

Kehat, I.; Kenyagin-Karsenti, D.; Snir, M.; Segev, H.; Amit, M.; Gepstein, A.; Livne, E.; Binah, O.; Itskovitz-Eldor, J. & Gepstein, L. (2001). Human embryonic stem cells can differentiate into myocytes with structural and functional properties of cardiomyocytes. *Journal of Clinical Investigation*; 108:407-14

Lasser, K. E.; Allen, P. D.; Woolhandler, S. J.; Himmelstein, D. U.; Wolfe, S. M. & Bohr D. H. (2002). Timing of new black box warnings and withdrawals for prescription medications. *JAMA*; 287(17):2215-20

Leor, J.; Aboulafia-Etzion, S.; Dar, A.; Shapiro, L.; Barbash, I. M.; Battler, A.; Granot, Y. & Cohen, S. (2000). Bioengineered cardiac grafts a new approach to repair the infarcted myocardium? *Circulation*; 102:III56–IIII61

Li, R. K.; Yau, T. M.; Weisel, R. D.; Mickle, D. A.; Sakai, T.; Choi, A. & Jia, Z. Q. (2000). Construction of a bioengineered cardiac graft. *Journal of Thoracic and Cardiovascular Surg*ery;119:368–375

Lo, Y. C.; Yang, S. R.; Huang, M.H.; Liu, Y. C. & Wu, S. N. (2005). Characterization of chromanol 293B-induced block of the delayed-rectifier K+ current in heart-derived H9c2 cells. *Life Sciences*;76:2275-2286

Naito, H.; Melnychenko, I.; Didie, M.; Schneiderbanger, K.; Schubert, P.; Rosenkranz, S.; Eschenhagen, T. & Zimmermann, W. H. (2006). Optimizing engineered heart tissue for therapeutic applications as surrogate heart muscle. *Circulation*; 114:I72–I78

Ott, H.C.; Matthiesen, T. S.; Goh, S. K.; Black, L. D.; Kren, S. M.; Netoff, T. I. & Taylor, D. A. (2008). Perfusion-decellularized matrix: using nature's platform to engineer a bioartificial heart. *Nature Medicine*; 14:213–221

Radisic, M.; Park, H.; Shing, H.; Consi, T.; Schoen, F. J.; Langer, R.; Freed, L. E. & Vunjak-Novakovic, G. (2004). Functional assembly of engineered myocardium by electrical stimulation of cardiac myocytes cultured on scaffolds. *PNAS*; 101:18129–18134

Ray, W. A.; Murray, K. T.; Meredith, S.; Narasimhulu, S. S.; Hall K. & Stein C. M. (2004). Oral erythromycin and the risk of sudden death from cardiac causes. *The New England Journal of Medicine*; 351(11):1089-96

Redfern, W. S.; Carlsson, L.; Davis, A. S.; Lynch, W. G.; MacKenzie I.;Palethorpe, S.; Siegl, P. K.; Strang, I.; Sullivan, A. T.; Wallis, R.; Camm, A. J. & Hammond, T. G. (2003). Relationship between preclinical cardiac electrophysiology, clinical QT interval prolongation and torsade de pointes for a broad range of drugs: evidence for a provisional safety margin in drug development. *Cardiovascular Research*; 58(1):32-45.

Regan, C. P.; Cresswell, H. K.; Zhang, R. & Lynch J. J. (2005). Novel method to assess cardiac electrophysiology in the rat. *Journal of Cardiovascular Pharmacology*; 46(1):68-75.

Shimizu, T.; Yamato, M.; Isoi, Y.; Akutsu, T.; Setomaru, T.; Abe, K.; Kikuchi, A.; Umezu, M. & Okano, T. (2002). Fabrication of pulsatile cardiac tissue grafts using a novel 3-dimensional cell sheet manipulation technique and temperature-responsive cell culture surfaces. *Circulation Research*; 90:e40

Vandenburgh, H.; Shansky, J.; Benesch-Lee, F.; Barbata, V.; Reid, J.; Thorrez, L.; Valentini, R. & Crawford, G. (2008). Drug-screening platform based on the contractility of tissue-engineered muscle. *Muscle Nerve*; 37:438-447

Vaughan-Williams E., M. (1975). Classificationof antidysrhythmic drugs. Pharmacology & therapeutics; 1(1):115-38.

Zhang, J.; Wilson, G. F.; Soerens, A. G.; Koonce, C. H.; Yu, J.; Palecek S. P.; Thomson J. A. & Kamp, T. J. (2009). Functional cardiomyocytes derived from human induced pluripotent stem cells. *Circulation Research*; 104:e30-41

Zimmermann, W. H.; Schneiderbanger, K.; Schubert, P.; Didie, M.; Munzel, F.; Heubach, J. F.; Kostin, S.; Neuhuber, W. L. & Eschenhagen, T. (2002). Tissue engineering of a differentiated cardiac muscle construct. *Circulation Research*; 90:223–230

Zimmermann, W. H.; Melnychenko, I.; Wasmeier, G.; Didié, M.; Naito, H.; Nixdorff, U.; Hess, A.; Budinsky, L.; Brune, K.; Michaelis, B.; Dhein, S.; Schwoerer, A.; Ehmke, H. & Eschenhagen, T. (2006). Engineered heart tissue grafts improve systolic and diastolic function in infarcted rat hearts. *Nature Medicine*; 12:452-8

Zimmermann, W. H. & Eschenhagen, T. (2007). Embryonic stem cells for cardiac muscle engineering. *Trends in Cardiovascular Medicine*; 17:134-40

Toxicity and Drug Testing

Edited by Prof. Bill Acree

Modern drug design and testing involves experimental in vivo and in vitro measurement of the drug candidate's ADMET (adsorption, distribution, metabolism, elimination and toxicity) properties in the early stages of drug discovery. Only a small percentage of the proposed drug candidates receive government approval and reach the market place. Unfavorable pharmacokinetic properties, poor bioavailability and efficacy, low solubility, adverse side effects and toxicity concerns account for many of the drug failures encountered in the pharmaceutical industry. Authors from several countries have contributed chapters detailing regulatory policies, pharmaceutical concerns and clinical practices in their respective countries with the expectation that the open exchange of scientific results and ideas presented in this book will lead to improved pharmaceutical products.